

Life and times of dwarf spheroidal galaxies

Stefania Salvadori¹, Andrea Ferrara¹ & Raffaella Schneider²

¹*SISSA/International School for Advanced Studies, Via Beirut 4, 34100 Trieste, Italy*

²*INAF/Osservatorio Astrofisico di Arcetri, Largo Enrico Fermi 5, 50125 Firenze, Italy*

ABSTRACT

We propose a cosmological scenario for the formation and evolution of dwarf spheroidal galaxies (dSphs), satellites of the Milky Way (MW). An improved version of the semi-analytical code GAMETE (Galaxy Merger Tree & Evolution) is used to follow the dSphs evolution simultaneously with the MW formation, matching the observed properties of both. In this scenario dSph galaxies represent fossil objects virializing at $z = 7.2 \pm 0.7$ (i.e. in the pre-reionization era $z > z_{rei} = 6$) in the MW environment which at that epoch has already been pre-enriched up to $[\text{Fe}/\text{H}] \sim -3$; their dynamical masses are in the narrow range $M = (1.6 \pm 0.7) \times 10^8 M_\odot$, although a larger spread might be introduced by a more refined treatment of reionization. Mechanical feedback effects are dramatic in such low-mass objects, causing the complete blow-away of the gas ~ 100 Myr after the formation epoch: 99% of the present-day stellar mass, $M_* = (3 \pm 0.7) \times 10^6 M_\odot$, forms during this evolutionary phase, i.e. their age is > 13 Gyr. Later on, star formation is re-ignited by returned gas from evolved stars and a second blow-away occurs. The cycle continues for about 1 Gyr during which star formation is intermittent. At $z = 0$ the dSph gas content is $M_g = (2.68 \pm 0.97) \times 10^4 M_\odot$. Our results match several observed properties of Sculptor, used as a template of dSphs: (i) the Metallicity Distribution Function; (ii) the Color Magnitude Diagram; (iii) the decrement of the stellar $[\text{O}/\text{Fe}]$ abundance ratio for $[\text{Fe}/\text{H}] > -1.5$; (iv) the dark matter content and the light-to-mass ratio; (v) the HI gas mass content.

Key words: stars: formation, population II, supernovae: general - cosmology: theory - galaxies: evolution, stellar content -

1 BACKGROUND

The lack of a comprehensive scenario for the formation and evolution of dwarf spheroidal galaxies (dSphs) contrast with the large amount of available data for these nearby Local Group satellites. Several authors have focused on different aspects of the dSph evolution and on the observed properties related with them, giving important contributions to our actual understanding of such puzzling objects. However, many questions remain unanswered and models able to match simultaneously different observed properties are still missing.

Recent observations by Helmi et al. (2006) opened new questions on the origin of dSph galaxies. By observing the stellar Metallicity Distribution Function (MDF) in four nearby dSphs, they found a significant lack of stars with $[\text{Fe}/\text{H}] < -3$. On the contrary, the Galactic halo MDF shows a low $[\text{Fe}/\text{H}]$ -tail extending down to $[\text{Fe}/\text{H}] \sim -4$ (Beers & Christlieb 2006) and even below (Christlieb et al. 2002, 2006; Frebel et al. 2005, Christlieb 2007). Does such result imply that dSph and MW progenitors are different? Is the dSph birth environment pre-enriched or does the Initial Mass Function (IMF) behave differently in Galactic building

blocks and in dSphs at earliest times? If the pre-enrichment can solve the problem it must be completed before the beginning of the star formation (SF) in dSphs i.e. > 13 Gyr ago. The dSph star formation histories (SFH) derived by the analysis of the observed color-magnitude diagram (CMD), in fact, show that all dSph have an ancient stellar population formed more than 13 Gyr ago (Grebel & Gallagher 2004). Which mechanism can be responsible of such rapid metal-enrichment?

In addition to these new open questions there is still a crucial unresolved problem related to the dSph's SFHs. In fact, although all dSphs display an ancient stellar population, their SFHs appear to be considerably different. In most of them the bulk of stars is made by ancient stars (> 10 Gyr old) i.e. their SF activity is concentrated during the first Gyrs (Dolphin et al. 2005). However Fornax, LeoII and Sagittarius show very different features: in these objects the bulk of the stars was formed much less than 10 Gyr ago and their SF activity proceeds until $z \sim 1$, or even to lower redshifts (Grebel & Gallagher 2004). Carina, finally, exhibits a clearly episodic SFH, with a pause of sev-

eral Gyrs after the old population formed and a massive formation of stars younger than 10 Gyr (Smecker-Hane et al. 1994, Hurley-Keller, Mateo & Grebel 1999). As pointed out by Grebel & Gallagher (2004) such variety of SFHs cannot be explained with a drop in the SF activity in response to photoionization; only Carina in fact displays the gap expected if the SF were truncated during reionization and then restarted. If reionization cannot explain the inferred variety of SFHs, local processes, such as mechanical feedback, tidal stripping, gas infall etc., must be invoked in order to produce these observational features. However, it is difficult that local processes can lead to different SFHs if the dSph host halo mass has a "Universal" value, as predicted by Mateo et al. (1998), Gilmore et al. (2007) and Walker et al. (2007), and if the assumed initial gas-to-mass ratio is taken to be equal to the cosmic mean value. Will more sophisticated observations and analysis reveal a spread in the dSph DM content? If this is the case, different host halo mass could be more easily linked to different SFHs by internal physical processes. In addition to these issues there are a number of related aspects that deserve attention, as for example the observed elemental abundance patterns (like the $[\alpha/\text{Fe}]$ ratio and the s-elements abundance).

Despite all of these unresolved questions, the relevance of stellar feedback for the evolution of dSph galaxies (Ferrara & Tolstoy 2002 and references therein) can be considered a milestone of our actual understanding of these objects, given the general consensus among theoretical studies and the continuous confirmation by observational evidences. Given their low DM content and therefore their shallow potential wells, mechanical feedback driven by SN explosions has dramatic effects in dSphs. Such intense mechanical feedback activity is indirectly confirmed by the low light-to-dark matter ratios observed in dSphs (Mateo et al. 1998, Gilmore et al. 2007). Moreover, observations of neutral hydrogen (HI), reveal that the Local Group dSphs are all relatively HI poor, suggesting that maybe most of the gas have been removed from these galaxies. The Sculptor dSph is one of the few with HI emission; a lower limit of $M_{\text{HI}} > 3 \times 10^4 M_{\odot}$ has been derived by Carignan et al. (1998) using radio observations. In addition, winds are presumably metal-enhanced, as suggested by several theoretical studies (Vader 1998; MacLow & Ferrara 1999; Fujita et al. 2004) and by recent X-rays observations of the starburst galaxy NGC 1569 (Martin, Kobulnicky & Heckman 2002).

Many theoretical works have attacked some aspects of the dSph evolution separately:

- Origin & DM content of dSphs: Bullock et al. (2001); Kravtsov et al. (2004); Ricotti & Gnedin (2005); Gnedin & Kravtsov (2006); Read, Pontzen & Viel (2006); Moore et al. (2006); Metz & Kroupa (2007).
- DSph MDFs: Ripamonti et al. (2006); Lanfranchi & Matteucci (2007)
- SFH & abundance ratios of dSphs: Ikuta & Arimoto (2002); Fenner et al. (2006); Lanfranchi & Matteucci (2007); Stinson et al. (2007).
- Stellar feedback & dSph gas content: Ferrara & Tolstoy (2000); Tassis et al. (2003); Fujita et al. (2004); Lanfranchi & Matteucci (2007).

In this study we analyze the formation and evolution of dSph galaxies, satellites of the MW, in their cosmological

context by using the improved Galaxy MErger Tree & Evolution code (GAMETE), which allows to build-up the SFH and chemical enrichment of the MW along its hierarchical merger tree (Salvadori, Schneider & Ferrara 2007, hereafter SSF07). This approach gives a self-consistent description of the dSphs evolution and MW formation: dSphs form out from their natural birth environment, the Galactic Medium (GM), whose metallicity evolution is completely determined by the history of SF and by mechanical feedback processes along the build-up of the Galaxy. The star formation and mechanical feedback efficiencies of dSphs are assumed to be the same as for all the Galactic building blocks and calibrated to reproduce the observable properties of the MW. The model allows to predict the following observable properties of a typical dSph galaxy: (i) the formation epoch; (ii) the MDF; (iii) the SFH and the derived CMD diagram; (iv) the stellar $[\text{O}/\text{Fe}]$ abundance ratio with respect to $[\text{Fe}/\text{H}]$; (v) the DM content; (vi) the stellar-to-mass ratio; (vii) the final gas content. These are compared with observations of Sculptor, which represents the best studied nearby dSph. A global scenario for the formation and evolution of dSph galaxies is presented.

The plan of the paper is the following: a recap of the general properties of the improved code GAMETE is presented in Sec. 2. The life of a dSph galaxy is described in subsequent sections: the birth environment and the selection criteria from the MW building blocks are presented in Sec. 3; the evolution until the blow-away, driven by mechanical feedback, is described in Sec. 4; the subsequent and final stages of the dSph life are traced in Sec. 5. Sec. 6 is devoted to a comparison between model results and some observational properties of the Sculptor dSph. Finally, a summary and discussion of the main results is given in Sec. 7.

2 MODEL DESCRIPTION

In this Section, we first summarize the main features of the model introduced in SSF07; following that we discuss the modifications and improvements made for the purpose of this work.

2.1 Summary of the model

The semi-analytic code GAMETE used in SSF07 allows to follow the star formation history and chemical enrichment of the MW throughout its hierarchical merger tree. Its main features can be summarized along the following points (for detailed explanations see SSF07). The code reconstructs the hierarchical merger history of the MW using a Monte Carlo algorithm based on the extended Press & Schechter theory (Bond et al. 1991; Lacey & Cole, 1993); it adopts a *binary* scheme with *accretion* (Cole et al. 2000, Volonteri, Haardt & Madau 2003) to decompose the present day MW dark matter halo ($M_{\text{MW}} \sim 10^{12} M_{\odot}$ Binney & Merrifield 1998) into its progenitors, running backward in time up to $z = 20$. At any time a halo of mass M_0 can either loose part of its mass (corresponding to a cumulative fragmentation into haloes with $M < M_{\text{res}}$) or loose mass and fragment into two progenitor haloes with random masses in the range $M_{\text{res}} < M < M_0/2$. The mass below the resolution limit accounts for the *Galactic Medium* (GM) which represents the mass

reservoir into which haloes are embedded. During the star formation history of the MW, the progenitor haloes accrete material from the GM and virialize out of it. We assume that feedback effects rapidly suppress star formation in the first mini-haloes and that only Ly α cooling haloes ($T_{vir} > 10^4$ K) contribute to the star formation history and chemical enrichment of the Galaxy. This motivates our choice of a resolution mass $M_{res} = M_4(z)/10$, where

$$M_4(z) = M(T_{vir} = 10^4 \text{ K}, z) \sim 10^8 M_\odot \left(\frac{10}{1+z} \right)^{3/2} \quad (1)$$

represents the halo mass corresponding to a virial equilibrium temperature $T_{vir} = 10^4$ K at a given redshift z . At the highest redshift of the simulation, $z \approx 20$, the gas present in virialized haloes is assumed to be of primordial composition. The star formation rate is taken to be proportional to the mass of gas. Following the critical metallicity scenario (Bromm et al. 2001; Omukai 2000, Omukai et al. 2005; Schneider et al. 2002, 2003, 2006; Bromm & Loeb 2004) we assume that low-mass star formation is triggered by the presence of metals (and dust) exceeding $Z_{cr} = 10^{-5 \pm 1} Z_\odot$. When the gas in star forming haloes has a metallicity $Z \leq Z_{cr}$ Pop III stars form with a reference mass value of $m_{popIII} = 200 M_\odot$. If on the contrary $Z > Z_{cr}$, Pop II/I stars form according to a Larson initial mass function (IMF):

$$\Phi(m) = \frac{dN}{dm} \propto m^{-1+x} \exp(-m_{cut}/m), \quad (2)$$

with $x = -1.35$, $m_{cut} = 0.35 M_\odot$ and m in the range $[0.1 - 100] M_\odot$ (Larson 1998). Due to the lack of spatial information, when metals and gas are returned to the interstellar medium (ISM) through stellar winds and SN explosions, they are assumed to be instantaneously and homogeneously mixed with the ISM. The same instantaneous perfect mixing approximation is applied to material ejected out of the host halo into the external GM.

2.2 New features

We now discuss the additional features we have incorporated in the model. The aim of introducing these new physics is to obtain a more complete description of the evolution of a single dSph galaxy. These can be summarized as follows:

- *Infall rate.* The gas in newly virialized haloes is accreted with an infall rate given by

$$\frac{dM_{inf}}{dt} = A \left(\frac{t}{t_{inf}} \right)^2 \exp \left(-\frac{t}{t_{inf}} \right). \quad (3)$$

The selection of this particular functional form has been guided by the results of simulations presented in Kereš et al. (2005). For reasons that will be clarified in Sec. 6.1, the infall time is assumed to be proportional to the free-fall time, $t_{inf} = t_{ff}/4$ where $t_{ff} = (3\pi/32G\rho)^{1/2}$, G is the gravitational constant, and ρ is the total (dark + baryonic) mass density of the halo. The normalization constant is set to be $A = 2(\Omega_b/\Omega_M)M/t_{inf}$ so that for $t \rightarrow \infty$ the accreted gas mass reaches the universal value $M_{inf}(\infty) = (\Omega_b/\Omega_M)M$. No infall is assumed after a merging event i.e. all the gas is supposed to be instantaneously accreted. Hydrodynamical simulations in fact show that galaxy mergers can drive significant inflow of gas raising the star formation rate by more

than an order of magnitude (Mihos & Hernquist, 1996 and references therein).

- *Finite stellar lifetimes.* We follow the chemical evolution of the gas taking into account that stars of different masses evolve on characteristic time-scales (Lanfranchi & Matteucci 2007). The rate at which gas is returned to the ISM through winds and SN explosions is computed as:

$$\frac{dR(t)}{dt} = \int_{m_1(t)}^{100 M_\odot} (m - w_m(m)) \Phi(m) SFR(t - \tau_m) dm, \quad (4)$$

where $\tau_m = 10/m^2$ Gyr is the lifetime of a star with mass m , w_m is the remnant mass and $m_1(t)$ the turnoff mass i.e. the mass corresponding to $t = \tau_m$. Similarly, the total ejection rate of an element i , newly synthesized inside stars (first term in the parenthesis) and re-ejected into the ISM without being re-processed (second term), is

$$\frac{dY_i(t)}{dt} = \int_{m_1(t)}^{100 M_\odot} [(m - w_m(m) - m_i(m, Z)) \times \quad (5)$$

$$Z_i(t - \tau_m) + m_i(m, Z)] \Phi(m) SFR(t - \tau_m) dm,$$

where $m_i(m, Z)$ is the mass of element i produced by a star with initial mass m and metallicity Z and $Z_i(t - \tau_m)$ is the abundance of the i -th element at the time $t - \tau_m$. The SN rate is simply computed as

$$\frac{dN_{SN}(t)}{dt} = \int_{m_1(t) > 8 M_\odot}^{40 M_\odot} \Phi(m) SFR(t - \tau_m) dm. \quad (6)$$

We used the grid of values $w_m(m)$ and $m_i(m, Z)$ by Heger & Woosley (2002) for $140 M_\odot < m < 260 M_\odot$, Woosley & Weaver (1995) for $8 M_\odot < m < 40 M_\odot$ and van der Hoek & Groenewegen (1997) for $0.9 M_\odot < m < 8 M_\odot$.

- *Mechanical feedback.* Assuming a continuous mass loss prescription (Larson 1974), the mass of gas ejected into the surrounding GM is regulated by the equation,

$$\frac{1}{2} M_{ej} v_e^2 = E_{SN} \quad (7)$$

where

$$E_{SN} = \epsilon_w N_{SN} \langle E_{SN} \rangle \quad (8)$$

is the kinetic energy injected by SN-driven winds and $v_e^2 = GM/r_{vir} = 2E_b/M$ is the escape velocity of the gas from a halo with mass M and binding energy E_b given by (Barkana & Loeb 2001)

$$E_b = \frac{1}{2} \frac{GM^2}{r_{vir}} = 5.45 \times 10^{53} \text{ erg} \left(\frac{M_8}{h^{-1}} \right)^{5/3} \left(\frac{1+z}{10} \right) h^{-1}.$$

In eq. 8, ϵ_w is a free parameter which controls the conversion efficiency of SN explosion energy in kinetic form, N_{SN} is the number of SN, and $\langle E_{SN} \rangle$ is the average explosion energy; the latter quantity is taken to be equal to 2.7×10^{52} erg for Pop III stars and to 1.2×10^{51} erg for Type II SNe. Differentiating eq. 7 we find that the gas ejection rate is proportional to the SN explosion rate,

$$\frac{dM_{ej}}{dt} = \frac{2\epsilon_w \langle E_{SN} \rangle}{v_e^2} \frac{dN_{SN}}{dt}. \quad (9)$$

- *Differential winds.* The gas ejected out of the host halo is assumed to be metal-enhanced with respect to the star forming gas. According to Vader (1986), who studied SN-driven gas loss during the early evolution of elliptical galax-

ies, the SN ejecta suffer very limited mixing before they leave the galaxy, playing a minor role in its chemical evolution. Such hypothesis implies different ejection efficiency for gas and metals. This result has been later confirmed by numerical studies (Mac Low & Ferrara, 1999; Fujita et al. 2004). Adopting a simple prescription, we assume that the abundance of the i -th element in the wind is proportional to its abundance in the ISM, $Z_i^w = \alpha Z_i^{ISM}$, and we take $\alpha = 10$ only for newly virialized haloes ($M < 10^9 M_\odot$) otherwise $\alpha = 1$.

For any star forming halo of the MW hierarchy, we therefore solve the following system of differential equations:

$$\frac{dM_*}{dt} = SFR = \epsilon_* \frac{M_g}{t_{ff}}, \quad (10)$$

$$\frac{dM_g}{dt} = -SFR + \frac{dR}{dt} + \frac{dM_{inf}}{dt} - \frac{dM_{ej}}{dt}, \quad (11)$$

$$\frac{dM_{Z_i}}{dt} = -Z_i^{ISM} SFR + \frac{dY_i}{dt} + Z_i^{vir} \frac{dM_{inf}}{dt} - Z_i^w \frac{dM_{ej}}{dt}. \quad (12)$$

The first equation is the star formation rate; M_g is the mass of cold gas inside haloes, ϵ_* the free parameter which controls the star formation efficiency and t_{ff} the free-fall time. The second equation describes the mass variation of cold gas: it increases because of gas infall and/or returned from stars and decreases because of star formation and gas ejection into the GM. The third equation, analogous to the second one, regulates the mass variation of an element i ; Z_i^{ISM} , Z_i^{vir} , and Z_i^w are the abundance of the i -th element in the ISM, in the infalling gas (i.e. in the hot gas at virialization), and in the wind, respectively.

2.3 Model parameters

The model has six free parameters: ϵ_* , ϵ_w , Z_{cr} , m_{PopIII} , t_{inf} and α . We use the observed global properties of the MW in order to fix ϵ_w and ϵ_* . To do so we compare the results of the simulations at redshift $z = 0$ with: (i) the gas metallicity $Z_{gas} \sim Z_\odot$; (ii) the stellar metallicity $Z_* \sim Z_\odot$; (iii) the stellar mass $M_* \sim 6 \times 10^{10} M_\odot$; (iv) the gas-to-stellar mass ratio $M_g/M_* = 0.1$; (v) the baryon-to-dark matter ratio $f_b = 0.07$; (vi) the GM metallicity $Z_{GM} \sim 0.25 Z_\odot$. The last quantity has been estimated using the observed value for [O/H] in high-velocity clouds (Ganguly et al. 2005) which are supposed to be gas leftover from the Galactic collapse and currently accreting onto the disk. The MDF of Galactic halo stars observed by Beers & Christlieb (2006) is instead used in order to fix the values of Z_{cr} and m_{PopIII} (Fig. 1, left panel). As we will discuss in detail in Sec. 6.1, the additional parameters t_{inf} and α are fixed to match the Sculptor MDF without altering the MW properties. Our fiducial model is characterized by the following parameters values*: $\epsilon_* = 1$, $\epsilon_w = 0.002$, $Z_{cr} = 10^{-3.8} Z_\odot$, $m_{PopIII} = 200 M_\odot$, $t_{inf} = t_{ff}(z_{vir})/4$ and $\alpha = 10$.

The comparison between the best-fitting model and the observed MDF is shown in the left panel of Fig. 1. The model

provides a good fit to the data; in particular, the selected Z_{cr} value allows to reproduce the peculiar MDF cut-off although it cannot account for the two isolated hyper iron-poor stars ([Fe/H] = -5.3 and [Fe/H] = -5.7) and for the recent observations of a star with [Fe/H] = -4.8 , the first detection in what was previously called “metallicity desert” (Christlieb 2007). These stars can only be reproduced assuming $Z_{cr} \leq 10^{-6} Z_\odot$, at the expenses of overpredicting the number of stars in the range $-5.3 < [\text{Fe}/\text{H}] < -4$, loosing the agreement with the observed MDF cut-off (see SSF07 for a detailed analysis of the dependence of the predicted MDF on Z_{cr} and m_{PopIII}). We find that most of the iron-poor stars ([Fe/H] < -2.5) form in haloes which originally contain gas of primordial composition but which accrete material from the GM, Fe-enhanced by previous SN explosions. The initial [Fe/H] abundance within a virializing halo is then fixed by the corresponding GM iron abundance at the virialization redshift. The evolution of GM iron and oxygen abundance predicted by the fiducial model is also shown in Fig. 1 (middle panel).

3 THE BIRTH ENVIRONMENT

Once the fiducial model has been fixed, its parameters are used to solve the system of equations (10)-(12) for *all* the progenitor haloes of the MW. The next point to address is the selection criteria to identify dSph galaxies among various MW progenitors. We use two criteria: the first is based on dynamical arguments and the second on reionization.

We want to select virializing haloes which could become dSph satellites. Using N-body cosmological simulations, Diemand, Madau & Moore (2005) show that in present-day galaxies, haloes corresponding to rare high- $\sigma(M, z)$ density peaks[†] are more centrally concentrated. The probability of a protogalactic halo to become a satellite increases if it is associated with lower- σ density fluctuations. This result, combined with the fact that at each redshift 95% of the total dark matter lies in haloes with mass $M < M_{2\sigma}$, which correspond to $< 2\sigma$ fluctuations, suggest that most satellites originate from such density peaks. Therefore, we select dSph candidates from haloes with masses $M_4 < M < M_{2\sigma}$. In Fig. 1 (right panel) we show the redshift evolution of $M_4(z)$, defined in eq. 1 as $M_4(z) = 10^8 M_\odot [(1+z)/10]^{-3/2}$, and of the halo masses corresponding to $1-3 \sigma(M, z)$ density peaks. Note that, in addition, the adopted dynamical criterion can be used to set an upper limit to the dSph candidates formation epoch of $z_{vir} < 9$ (see Fig. 1, right panel).

The second criterion is based on reionization. During this epoch, the increase of the Inter Galactic Medium (IGM) temperature causes the growth of the Jeans mass and consequent suppression of gas infall in low-mass objects. In particular, cosmological simulations by Gnedin (2000) show that below a characteristic halo mass-scale the gas fraction is drastically reduced compared to the cosmic value. We adopt a simple prescription and assume that after reionization the formation of galaxies with circular velocity $v_c < 30$ km/s

* The difference of ϵ_* , ϵ_w values with respect to those found in SSF07 is a result of model improvements. Note however that the integrals of the star formation rate and the gas ejection rate from progenitor haloes remain unaltered.

[†] The quantity $\sigma(M, z)$ represents the linear theory rms density fluctuations smoothed with a top-hat filter of mass M at redshift z .

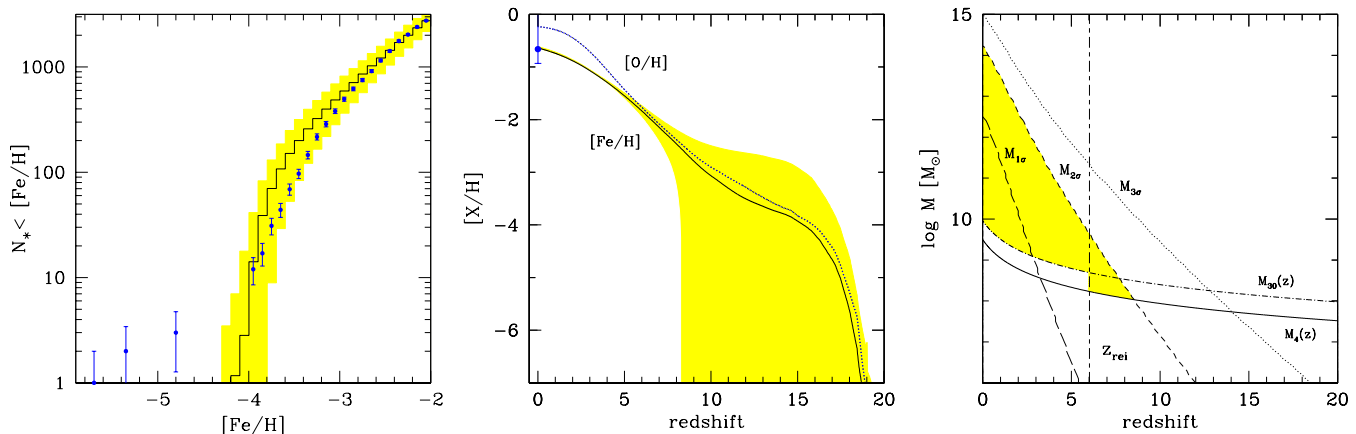


Figure 1. *Left panel:* Cumulative number of stars below a given $[\text{Fe}/\text{H}]$ observed by Beers & Christlieb (2006) in the Galactic halo, with the inclusion of the three hyper-iron poor stars (Christlieb et al. 2002, 2006; Frebel et al. 2005, Christlieb 2007) (points), and simulated by using the fiducial model (histogram). The histogram is the average value over 100 realizations of the merger tree re-normalized to the number of observed stars with $[\text{Fe}/\text{H}] \leq -2$. The shaded area represents $\pm 1\sigma$ errors. *Middle:* Evolution of GM iron (solid line) and oxygen (dotted line) abundance. Lines are the average values over 100 realizations of the merger tree. The shaded area delimits the $\pm 1\sigma$ dispersion region for $[\text{Fe}/\text{H}]$. The point is the measured $[\text{O}/\text{H}]$ in high-velocity clouds (Ganguly et al. 2005). *Right:* Evolution of the mass corresponding to 1 (long dashed line), 2 (short dashed line) and $3\sigma(M, z)$ (dotted line) density peaks; the solid line show the evolution of $M_4(z)$ (eq.1), the dotted-dashed line the evolution of $M_{30}(z)$. The selected reionization redshift $z_{\text{rei}} = 6$ is also shown in the Figure. The shaded area delimits the region $M_4(z) < M < M_{2\sigma}$ for $z > z_{\text{rei}}$, $M_4(z) < M < M_{2\sigma}$ for $z < z_{\text{rei}}$.

is suppressed, i.e. we assume that when $z < z_{\text{rei}}$ haloes with masses below $M_{30}(z) = M(v_c = 30 \text{ km/s}, z)$ have no gas (for a thorough discussion of radiative feedback see Ciardi & Ferrara 2005 and Schneider et al. 2007). Since $M_{30}(z) > M_4(z)$ (see the right panel of Fig. 1) and the probability to form a newly virialized halo with $M > M_{30}$ is very low, the second criterion implies that the formation of dSph candidates is unlikely to occur below z_{rei} . As we will discuss in Sec. 6.4 this fact may have important consequences as, for example, the possible existence of a universal mass of dSph host haloes.

Following the two above criteria, dSph candidates can only form in the redshift range $z_{\text{rei}} < z_{\text{vir}} < 9$. From the middle panel of Fig. 1 it is evident that in this redshift range the mean GM iron abundance is $-2.5 \lesssim [\text{Fe}/\text{H}] \lesssim -3$. This implies that the birth environment of dSph candidates is pre-enriched to $[\text{Fe}/\text{H}]$ values consistent with those implied by the MDF observations of Helmi et al. (2006).

In what follows, we will present the results obtained by our fiducial model averaged over 100 different realizations of the hierarchical merger tree of the MW. In each single realization, dSph candidates are selected from haloes with masses and redshifts corresponding to the shaded area in the right panel of Fig. 1, that is $M_4 < M < M_{2\sigma}$ for $z > z_{\text{rei}}$ and $M_{30} < M < M_{2\sigma}$ otherwise. Their subsequent evolution is followed in isolation with respect to the forming Galaxy: they neither merge nor accrete material from the GM. Following Choudhury & Ferrara (2006), we vary the reionization redshift within the range $5.5 < z_{\text{rei}} < 10$. The total number of dSph candidates depends on z_{rei} and it is typically larger than the number of observed ones. Therefore, for each z_{rei} , it is necessary to randomly extract a sub-sample in order to match the total number of known MW satellites, ~ 15 . The average properties of a dSph galaxy presented in the following Sections refer to the case $z_{\text{rei}} = 6$ (see the discussion in Sec. 6.1) and are obtained averaging over the

selected satellites from all the 100 realizations of the MW merger tree (about ~ 2000 objects).

4 FEEDBACK-REGULATED EVOLUTION

The life of a dSph is very violent in the first hundred Myr, due to mechanical feedback effects which are more intense in low mass objects. The evolution of the mass of cold gas (eq. 11) helps in understanding this rapid evolution. Fig. 2 shows the evolution of several properties of an average dSph galaxy ($M = 1.6 \times 10^8 M_\odot$) that virialized at $z_{\text{vir}} = 7.2$, with respect to the formation time (age) $T = t - t_{\text{vir}}$. Three main evolutionary phases are identified in the Figure, depending on the dominant physical processes.

An increasing fraction of cold gas is collected during Phase I ($T < 40 \text{ Myr}$) dominated by the infall rate. The mass of the infalling gas rapidly increases during this epoch, reaching a maximum when $T = t_{\text{inf}} \sim 25 \text{ Myr}$. The mass of ejected and returned gas start to contribute to eq. (11) only when the most massive SNe of $40 M_\odot$ explode[†], $\sim 6 \text{ Myr}$ from the formation of the first stellar generation. Thereafter, the mass of ejected and returned gas rapidly grow, due the raising number of SNe and evolving low mass stars. The ISM metallicity and iron abundance evolve accordingly during this phase: they are steadily equal to the values of the infalling gas ($Z_{\text{vir}} \sim 10^{-3} Z_\odot$, $[\text{Fe}/\text{H}] \sim -2.9$) before the first SNe explodes and then rapidly increase.

During Phase II ($40 \text{ Myr} \lesssim T \lesssim 60 \text{ Myr}$) the gain of

[†] Stars with $40 M_\odot < m < 100 M_\odot$ are predicted to collapse to black holes (Woosley & Weaver, 1995) while massive Pop III stars cannot be produced in dSph galaxies since their birth environment is pre-enriched to $Z_{\text{vir}} \sim 10^{-3} Z_\odot > Z_{\text{cr}} = 10^{-3.8} Z_\odot$

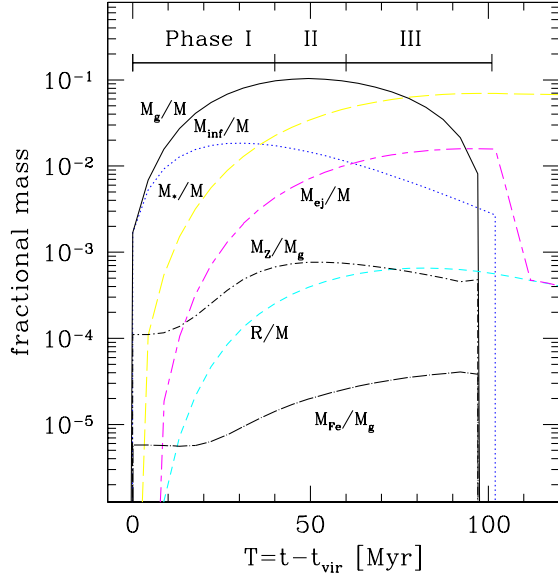


Figure 2. Evolution of M_g/M (solid line), M_*/M (long dashed line), M_{inf}/M (dotted line), M_{ej}/M (long-short dashed line), R/M (short dashed line), M_Z/M_g (dotted-short dashed line), M_{Fe}/M_g (dotted-long dashed line) for a typical dSph with total mass $M = 1.6 \times 10^8 M_\odot$, that virialize at redshift $z_{vir} = 7.2$, with respect to its age $T = t - t_{vir}$. The three main evolutionary phases (Phase I $T < 40$ Myr, Phase II $40 \text{ Myr} < T < 60$ Myr, Phase III $T > 60$ Myr) are also shown.

cold gas by infall is mostly used to form stars and M_g remains constant. Note that the M_*/M curve in Fig. 2 represents the *total* stellar mass at time T .

Finally, during Phase III ($T \gtrsim 70$ Myr), the mass of the ejected gas overcomes the infalling gas and M_g starts to decrease. Because of the metal-enhanced wind prescriptions M_Z and M_{Fe} should in principle decrease earlier and faster than M_g . This is the case for M_Z : in Fig. 2 the metallicity is a slowly decreasing function both during Phase II and Phase III so that $|\dot{M}_Z| < |\dot{M}_g|$. Conversely, the M_{Fe}/M_g ratio is enhanced during these epochs: the mass of newly synthesized iron released by a SN with a $m = 12 M_\odot$ progenitor is ~ 2 orders of magnitude bigger than for $m = 40 M_\odot$ (Woosley & Weaver, 1995)[§]; for this reason, when lower mass SNe evolve, a larger amount of iron is injected into the ISM and the second right-term in eq. 12 can contrast the high ejection rate.

When $T \sim 100$ Myr the mass of gas lost due to winds becomes larger than the remaining gas mass and M_g drops to zero. During this blow-away metals and iron are also ejected out of the galaxy. Moreover, since SN explosions continue at subsequent times, even the infalling gas can rapidly acquire enough energy to escape the galaxy. The infall is first reversed and in few Myr, when the remaining mass of hot gas has blown-away, definitively stopped. The occurrence of reversal infall in high-redshift dwarf galaxies is confirmed

[§] This result is virtually independent of the initial metallicity of the star. In the same mass range, the total mass of metals produced remains constant.

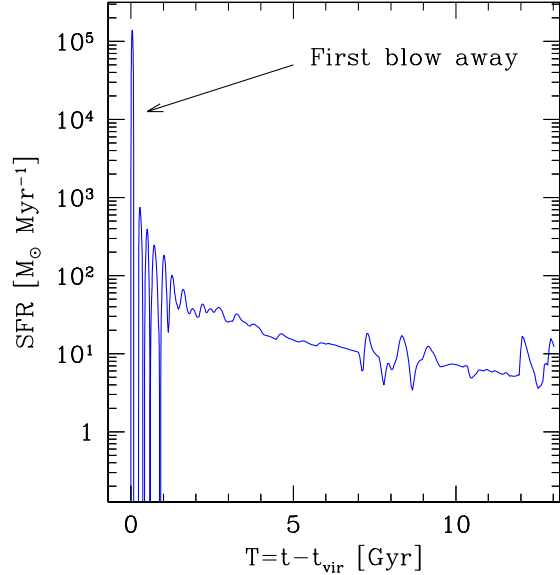


Figure 3. SFR of a typical dSph with total mass $M = 1.6 \times 10^8 M_\odot$, which virialize at redshift $z_{vir} = 7.2$, as a function of its age $T = t - t_{vir}$. The arrow shows the occurrence of the first blow-away.

by numerical simulations (Fujita et al. 2004). Eventually at $T \sim 100$ Myr our template dSph is a gas free system.

5 BEYOND BLOW-AWAY

In Fig. 3 we show the star formation rate (SFR) of a typical dSph galaxy as a function of its age. The highest peak corresponds to the star formation activity during the first 100 Myr i.e. before the blow away. After the blow-away the galaxy remains gas free and star formation is suddenly halted i.e. $SFR(T) = 0$. The gas returned by evolved stars represents the only source of fresh gas for the galaxy after the blow away. However, until the latest SN explodes, this low mass of gas is easily ejected outside the galaxy by SN winds (Fig. 2); the dSph remains dormant ($SFR = 0$) for the subsequent ~ 150 Myr (this time-lag corresponds to the life time of the lowest $m = 8 M_\odot$ SN progenitor formed just before the blow-away). Observationally, mass loss from evolved stars has been invoked by Carignan et al. (1998) in order to explain the detection of neutral hydrogen (HI) associated with the Sculptor dSph galaxy.

After the latest SN explosion, the return rate dR/dt by evolved stars with $m < 8 M_\odot$ becomes the only non-zero term of eq. 11 and the dSph enters a rejuvenation phase: the recycled gas is collected into the galaxy and star formation starts again.

From the beginning of the rejuvenation phase the subsequent evolution of the galaxy proceeds like in the first 100 Myr of its life. However (Fig. 3) SFR is now more than 2 orders of magnitude lower than before the first blow-away, due to the paucity of returned gas. Almost 100 Myr later the galaxy is drained of the whole mass of gas and metals: a new blow-away has occurred and the cycle starts again.

In Fig. 3 we note that the repetition of blow-away and

rejuvenation phases causes an intermittent SF activity with a typical blow-away separation of ~ 150 Myr. Such burst-like SFH is similar to that inferred from the CMD observed in dSph galaxies such as Carina (Smecker-Hane et al. 1994) although the typical duration of active and quiescent phases is $\sim (1-2)$ Gyr. In agreement with the present work, recent simulations for the collapse of an isolated dwarf galaxy (Stinson et al. 2007), show that feedback effects cause a periodic SF activity, with a typical duration of active and quiescent phases of ~ 300 Myr.

Fig. 3 also shows that about 1 Gyr after the formation of the galaxy, this burst-like SFH ends. Because of the gradually smaller mass of gas returned by stars, fewer SNe are produced during this epoch. For this reason, gas ejection is less efficient and can be easily counteracted by the continuous input of returned gas.

Although the SF activity continues until the present-day, the mass of stars formed after the first blow-away ($M_* \sim 2 \times 10^5 M_\odot$) is only 1% of the mass of stars formed before the blow-away ($M_* \sim 2 \times 10^7 M_\odot$). Consistent with this result, the analysis of the dSph CMD diagrams by Dolphin et al. (2005) shows that dSphs typically form most of their stars over 10 Gyr ago.

After the first blow-away subsequent stellar generations formed out of gas recycled by low mass star. The characteristic iron-abundance of this gas is $[\text{Fe}/\text{H}] \sim -1.5$, as can be inferred using the results of van der Hoek & Groenewegen (1997).

6 OBSERVABLE PROPERTIES

In the following Sections we will compare our numerical results for dSph galaxies with the most relevant observations. Given the amount of available data we take Sculptor as the best case of a dSph template; however, the validity of model results is general.

6.1 Metallicity distribution function

In this Section we analyze the Metallicity Distribution Function (MDF) of Sculptor, i.e. the number of relic stars as a function of their iron abundance $[\text{Fe}/\text{H}]$, a quantity commonly used as a metallicity tracer. In Fig. 4 we compare the MDF observed by Helmi et al. (2006) with the simulated one, normalized to the total number of observed stars (513). The theoretical MDF is obtained as follows: we adopt a reionization redshift of $z_{\text{rei}} = 6$; given this choice, the average number of dSph candidates in each realization is $N_{\text{tot}} \sim 200$, among which 10% become MW satellites, hence naturally matching the number of observed satellites. A higher reionization redshift of $z_{\text{rei}} = 8.5$ would reduce the number of dSph candidates to $N_{\text{tot}} \sim 5$, well below the observed value. This allows to put a solid constraint on the reionization redshift of $z_{\text{rei}} < 8.5$. As can be inferred from the Figure, the model shows a good agreement with the observed MDF, particularly for $[\text{Fe}/\text{H}] < -1.5$. A marginally significant deviation is present at larger $[\text{Fe}/\text{H}]$ values.

We have already discussed in the previous Section that the bulk of stars ($\sim 99\%$) in a dSph galaxy is formed during the first 100 Myr of its life when $[\text{Fe}/\text{H}] < -1.5$. Essentially, stars formed after the first blow away ($[\text{Fe}/\text{H}] > -1.5$), are

unnoticeable in the normalized MDF. For this reason the physical processes regulating the MDF shape are mostly those responsible for the cold gas mass evolution analyzed in Sec. 4. We can use the evolution of M_{Fe}/M_g shown in Fig. 2 in order to convert time in $[\text{Fe}/\text{H}]$ variable and identify the three main evolutionary phases into the MDF.

We find that stars with $[\text{Fe}/\text{H}] \lesssim -2$ formed during the infall-dominated Phase I; the MDF shape at low $[\text{Fe}/\text{H}]$ values is then essentially regulated by the functional form of the infall rate. Stars with $-2 \lesssim [\text{Fe}/\text{H}] \lesssim -1.6$ (around the MDF maximum) are formed during Phase II i.e. when the mass of cold gas remains approximately constant; the maximum of the MDF is instead fixed by the values of t_{inf} and α . In particular, t_{inf} determines the beginning of Phase II and α its end. Their values ($t_{\text{inf}} = t_{\text{ff}}(z_{\text{vir}})/4$, $\alpha = 10$) have been selected in order to match the Sculptor MDF maximum/shape without altering the global MW properties and Galactic halo MDF (the same parameter are in fact applied to all the virialized MW building blocks). Finally, stars with $[\text{Fe}/\text{H}] \gtrsim -1.6$, are formed during the feedback-dominated Phase III. Note in particular that the value of the MDF cut-off ($[\text{Fe}/\text{H}] \sim -1.5$) corresponds to the gas iron-abundance at the blow-away.

At $[\text{Fe}/\text{H}] \gtrsim -1.5$ our model slightly underpredicts the data as the theoretical MDF drops very steeply. The explanation for such disagreement is likely to reside in our simplified dynamical treatment of mechanical feedback. Interestingly, Mori, Ferrara & Madau (1999), investigated the dynamics of SN-driven bubbles in haloes with $M = 10^8 M_\odot$ at $z = 9$ using 3D simulations. They found that less than 30% of the available SN energy gets converted into kinetic energy of the blown away material, the remainder being radiated away. A large fraction of gas remains bound to the galaxy, but is not available to form stars before it cools and rains back onto the galaxy after ~ 200 Myr. Such effect is not included in our modeling. Qualitatively we do expect that such “galactic fountain” would increase the amount of Fe-enriched gas to restart SF after blow-away, and hence the number of $[\text{Fe}/\text{H}] \geq -1.5$ stars.

The total number of relic stars shown in the MDF corresponds to a total stellar mass of $M_* = (3 \pm 0.7) \times 10^6 M_\odot$. Using the total (dark+baryonic) dSph mass, derived from our simulations $M = (1.6 \pm 0.3) \times 10^8 M_\odot$ we can compute the mass-to-luminosity ratio

$$\left(\frac{M}{L_*}\right) = \left(\frac{M}{M_*}\right) \times \left(\frac{M_*}{L_*}\right) \sim 150 \quad , \quad (13)$$

having assumed $(M_*/L_*) = 3$, in agreement with the results by Ricotti & Gnedin 2005. This result is consistent with the most recent estimate for Sculptor (Battaglia 2007; Battaglia et al. 2008), that gives a very high value $(M/L) = 158 \pm 33$.

6.2 Color-magnitude diagram

Another comparison with data can be done in terms of color-magnitude diagram (CMD) of the Sculptor stellar population observed by Tolstoy et al. (2004). CMD represents one of the best tools to study the star formation history of a galaxy. Starting from our numerical results for a typical dSph, we have computed the corresponding synthetic CMD using the publicly available IAC-STAR code by Aparicio & Gallart (2004). Given the IMF, the SFR and the ISM

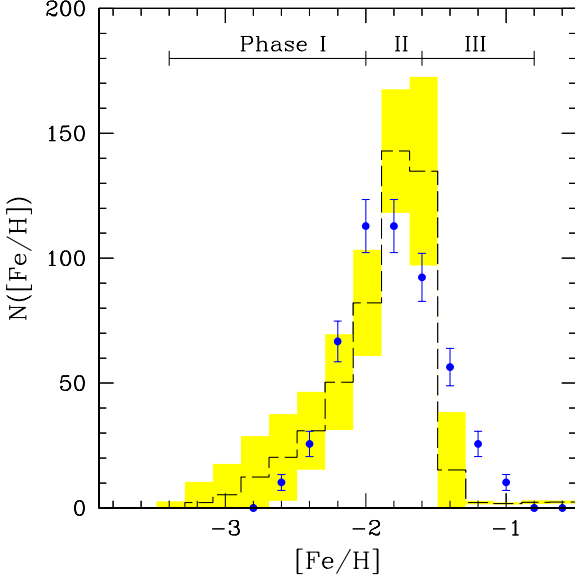


Figure 4. Comparison between the Sculptor MDF observed by Helmi et al. (2006), (points) and simulated one obtained by assuming $t_{inf} = t_{ff}/4$, $\alpha = 10$, $z_{rei} = 6$ (histogram). Error bars are the Poissonian errors. The histogram is the averaged dSph MDF over the surviving satellites (~ 20) in all the 100 realization of the merger tree (~ 2000 objects). The shaded area represents the $\pm 1\sigma$ Poissonian error.

metallicity evolution, IAC-STAR allows to calculate several properties of the relic stellar population and, in particular, the stellar magnitudes. We have used the stellar evolution library by Bertelli (1994) and the bolometric correction library by Lejeune et al. (1997). Note that the IAC-STAR input parameters for the ISM metallicity evolution must be $Z^{IAC-STAR} > 0.005Z_{\odot}$. No binary stars have been included.

We adopt a randomization procedure in order to simulate the observational errors in the synthetic CMD and compare numerical results with data. To this aim, we first derive the normalized error distribution for the magnitude M_I and the color index $V - I$ from the data sample by Tolstoy (private communication). Errors have been randomly assigned at every synthetic star, identified by a $(M_I, V - I)$ pair using a Monte Carlo method and randomly added or subtracted. Note that more accurate (and complicated) randomization procedures exist (see for example Aparicio & Gallart 2004); however, we consider the simple approach adopted here adequate for our present purposes. In Fig. 5 we compare the synthetic and observed CMDs. Data by Tolstoy et al. (~ 10300 stars into the relevant $M_I, V - I$ range) have been normalized to the total number of synthetic stars derived by IAC-STAR (~ 2300). In order to do so stars have been randomly selected from the data sample.

The match between theoretical and experimental points is quite good. We note however that the number of red giant branch (RGB) stars in the synthetic CMD is lower than the observed one. This discrepancy can be explained with the contamination of the data sample by Galactic foreground stars (see Tolstoy et al. 2004). The synthetic CMD reproduces reasonably well the blue/red horizontal branch stars

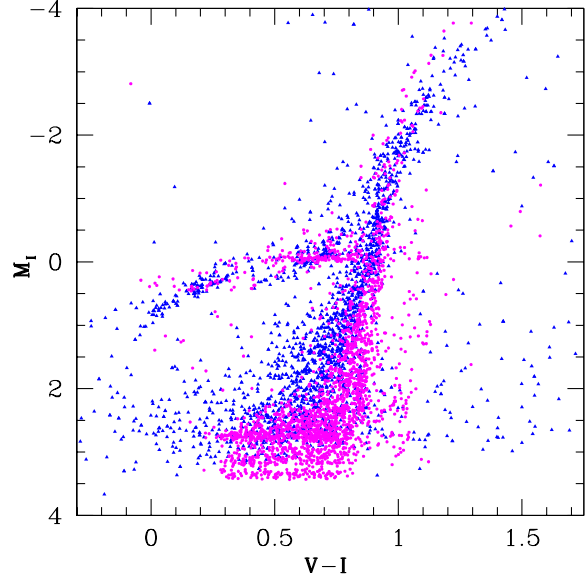


Figure 5. Comparison between the CMD of the Sculptor stellar population observed by Tolstoy et al. (2004) (triangles) and the synthetic CMD (open points) derived for a typical dSph galaxy with total mass $M = 1.6 \times 10^8 M_{\odot}$ which virialize at redshift $z_{vir} = 7.2$.

(BHB/RHB stars) i.e. stars residing in the CMD branch ($0 < M_I < 1$, $0 < (V - I) < 1$). A well populated HB in the CMD diagram might be interpreted as an indication of an old stellar population (age > 10 Gyr). The interpretation of the blue and red HB, on the contrary, is quite controversial: due to the age-metallicity degeneracy of the CMD stellar colors become bluer when stars are younger and/or poorer in metallicity. For this reason the position of a star in the CMD cannot be unequivocally interpreted. In our model the majority of the stars are formed during the first 100 Myr of the dSph life; this means that all the stars have basically the same age $\gtrsim 13$ Gyr; so the HB morphology, in our model, reflects the metallicity gradient of the stellar populations: BHB stars belong to metal-poor stars formed during the Phase I (see Fig. 2) while RHB stars to the more metal-rich stars formed during the Phase II.

6.3 Key abundance ratios

A method commonly used to break the age-metallicity degeneracy and derive accurate SFH from the CMD diagrams, is the analysis of the stellar elemental abundances. In most of the observed dSph galaxies the abundance ratio of α elements (O, Mg, Si, Ca) relative to iron ($[\alpha/Fe]$) shows a strong decrease when $[Fe/H] > -2$ (Venn et al. 2004). Since α -elements are primarily generated by SN II while a substantial fraction of iron-peak elements (Fe, Ni, Co) are produced by type Ia SNe (SNe Ia), the decline of $[\alpha/Fe]$ is usually interpreted as a contribution by SNe Ia. Using this argument and the assumption that the lifetime of SNe Ia is around 1.5 Gyr, Ikuta & Arimoto (2002) inferred an age spread of 1-2 Gyr in the dominant stellar population of Draco, Sextans and Ursa Minor dSphs. However, the issue of the lifetime of SNe Ia remains quite debated and uncertain, with timescales

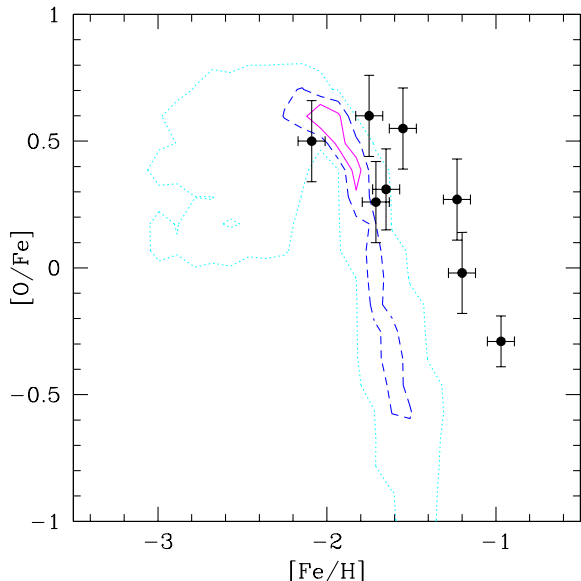


Figure 6. Oxygen-to-iron stellar abundance with respect to $[\text{Fe}/\text{H}]$ for the Sculptor dSph. Points refer to 8 Sculptor stars observed by Gaisler et al. (2005) and Shetrone et al. (2003); contours represent the probability, respectively equal to 0.6 and 0.8 and 0.99, to find a star into the $[\text{O}/\text{H}]-[\text{Fe}/\text{H}]$ plane.

as short as 40 Myr having been suggested (see Ricotti & Gnedin 2005 for a thorough discussion) under starburst formation conditions.

In Fig. 6 we compare the oxygen-to-iron stellar abundance with respect to $[\text{Fe}/\text{H}]$ for 8 stars observed in Sculptor by Gaisler et al. (2005) and Shetrone et al. (2003), with the results of our model. In spite of the poor statistics the data show a clear indication of the $[\text{O}/\text{Fe}]$ decrement for $[\text{Fe}/\text{H}] > -1.8$; in particular, subsolar values are observed. Even if SNe Ia are not included in our model, a drop in the $[\text{O}/\text{Fe}]$ occurs as a result of having released the IRA approximation (see also Fenner et al. 2006) and of differential winds. However, subsolar $[\text{O}/\text{Fe}]$ values can only be accounted for by differential winds. This is because when $[\text{O}/\text{Fe}]$ reaches the maximum value[¶], the “effective oxygen yield” ($dY_{\text{O}}/dt - Z_{\text{O}}^w dM_{\text{ej}}/dt$) is strongly reduced with respect to iron due the effect of differential winds, which, as can be deduced from eq. (12), have a larger impact on more abundant elements ($Z_i^w = \alpha Z_i^{\text{ISM}}$). This causes a pronounced and rapid decrease of $[\text{O}/\text{Fe}]$ to subsolar values. We note that model results tend to underpredict the observed stellar abundances: essentially, differential winds are too efficient. We recall, however, that the value $\alpha = 10$ have been selected in order to match the Sculptor MDF. The problem of the lack of $[\text{Fe}/\text{H}] > -1.5$ stars noted in Sec. 6.1, is evident also here. A more sophisticated treatment of differential winds and/or the inclusion of the missing physical effects discussed in Sec. 6.1, should presumably remove such discrepancies. Noticeably the result of Fig. 6 is fully consistent with the analysis by Fenner et al. (2006), who studied

[¶] The relative production rate of oxygen with respect to iron is larger in low-mass SNe II.

the Sculptor chemical evolution including differential winds. In conclusion we find that the trend of $[\alpha/\text{Fe}]$ does not require a prolonged star formation phase (> 1 Gyr) but can be satisfactorily explained even if 99% of the stars formed during the first 100 Myr of the dSph lifetime.

Additional constraints on the SFH may also come from the analysis of the abundances of s-elements associated with the slow neutron-capture process. These are produced by low-mass stars during Asymptotic Giant Branch (AGB) phases. From an analysis of $[\text{Ba}/\text{Y}]$ Fenner et al (2006) concluded that most of the stars must be formed over an interval of at least several Gyr to allow time for metal-poor AGB stars to enrich the ISM up to the observed values. Our model does not make specific prediction on s-elements; it is likely however that since the bulk of stars is predicted to be formed on a time-scale of ~ 100 Myr there would not be enough time for the ISM to be enriched with the products of AGB stars. Nevertheless this may not be the only scenario to explain s-elements abundances. For example binary systems in which the lower mass, long-living star, accretes s-enhanced gas directly from the companion rather than from the ISM can equally explain the observed high s-elements abundances. Internal production during the dredge-up phase can represent yet another possibility. These alternative scenarios are supported by the observed stellar $[\text{s}/\text{Fe}]$ ratio with respect to $[\text{Fe}/\text{H}]$. The data (Venn et al. 2004) show that the $[\text{s}/\text{Fe}]$ values do not increase at higher $[\text{Fe}/\text{H}]$, as expected if the ISM is gradually enriched by the contribution of lower mass stars. Moreover, a large $[\text{s}/\text{Fe}]$ spread is observed for any $[\text{Fe}/\text{H}]$ which is expected if the efficiencies of accretion, dredge-up and s-element production are functions of stellar mass.

6.4 Dark matter content

dSph galaxies represent the most dark matter-dominated systems known in the Universe. It is then very interesting to determine their dark matter mass. Observationally, the mass content of dSph galaxies is derived by measuring the velocity dispersion profile of their stellar populations and comparing it with the predictions from different kinematic models. The latter step strongly depends on the adopted stellar kinematics (in particular the assumed velocity anisotropy radial profile), on the dark matter mass distribution, and on the nature of the dark matter itself.

Recently, Battaglia (2007), Battaglia et al. (2008) have derived the velocity dispersion profile of Sculptor measuring the velocities of ~ 470 RGB stars. They model Sculptor as a two component system with a metal poor and a metal rich stellar population that show different kinematics. They use these two components as distinct tracers of the same potential and find that the best model is a cored profile with $r_c = 0.5 \text{ kpc}$ and $M(< r_{\text{last}})^{\parallel} = (3.4 \pm 0.7) \times 10^8 M_{\odot}$ which gives an excellent representation of the data assuming an increasing radial anisotropy. Interestingly, the values of $M(< r_{\text{last}})$ obtained assuming a NFW model for the dark matter distribution or a constant radial anisotropy are $M(< r_{\text{last}}) = (2.4_{-0.7}^{+1.1}) \times 10^8 M_{\odot}$ and $M(< r_{\text{last}}) = (3.3 \pm 0.8) \times 10^8 M_{\odot}$, respectively, consistent with the above result within 1σ .

^{||} $M(< r_{\text{last}})$ is the mass enclosed within the last measured point.

The average mass of dSph galaxies that we infer from our simulations, $M = (1.6 \pm 0.8) \times 10^8 M_\odot$. Because the last measured points in the Battaglia (2007), Battaglia et al. (2008) typically reach 1-2 kpc, one could suspect that additional dark matter could be located outside this radius, thus turning their determination into a lower mass limit. However, for the mean mass value and formation redshift that we have obtained $M \approx 10^8 M_\odot$, $z_{\text{vir}} \approx 7$, the virial radius of such a halo is 1 kpc. Thus, the agreement (at $1 - 2\sigma$ level) between our prediction and the actual mass determinations might not be coincidental, but reflects the fact that in these small objects star formation has propagated up to the most remote galactocentric regions. This prediction could be eventually checked by deeper observations and/or other techniques.

The narrow dispersion around the average mass value found is an indication that dSphs may have a universal host halo mass. This finding agrees with the results by Mateo et al. (1998), Gilmore et al. (2007) and Walker et al. (2007), who suggest that dSph galaxies might have a common mass scale $M_{0.6} = (2 - 7) \times 10^7 M_\odot$, where $M_{0.6}$ is the dark matter mass within a radius of 0.6 kpc. Assuming a NFW density profile, $z_{\text{vir}} = 0$ and a concentration parameter $c = 35$ (Battaglia 2007) we found $M_{0.6} = 2.3 \times 10^7 M_\odot$.

6.5 Gas footprints of feedback

A final comparison with data can be done in terms of the observed gas properties. In the previous Sections we have shown that metal-enhanced winds driven by SN explosions play a fundamental role in determining the evolutionary times scales and properties of a dSph galaxy. Based on observations obtained with the Chandra X-Ray Observatory, Martin, Kobulnicky & Heckman (2002) provide the first direct evidence for metal-enhanced winds from dwarf starburst galaxies. They have observed the hot X-ray-emitting gas around the nearby dwarf galaxy NGC 1569 which entered in a starburst phase (10-20) Myr ago. The X-ray spectrum they find presents strong emission lines from α -process elements, that require the wind metallicity to be $Z^w > 0.25 Z_\odot$ i.e. larger than $Z^{\text{ISM}} = 0.2 Z_\odot$, supporting our assumption of metal enhanced winds $Z^w = 10 Z^{\text{ISM}}$. In particular, their best fit models predict the ratio of α -elements to Fe to be 2-4 times higher than the solar value; it is then likely that the ISM is preferentially depleted in α -elements consistent with the findings shown in Fig. 6. We stress that these observations confirm the idea that mechanical feedback processes start to play a significant role in the dSph evolution on a very short time-scale (10-20 Myr after the beginning of the starburst phase).

Alternatively, the efficiency of mechanical feedback processes can be tested using observations of neutral hydrogen (HI). The Local Group dSph galaxies are all relatively HI poor (Mateo 1998) suggesting that little gas has remained after the main SF phase. Within the known dSph galaxies, Sculptor is one of the few with detectable HI emission. Using radio observation, Carignan et al. (1998) derived a lower limit for the HI mass of $M_{\text{HI}} > 3 \times 10^4 M_\odot$. Our simulation predicts an average mass of gas $M_g = (2.68 \pm 0.97) \times 10^4 M_\odot$, in very good agreement with the observed value if indeed this gas is in neutral form. According to our model, the HI mass detected in Sculptor can be associated to gas returned

by evolved stars, an explanation also offered by Carignan et al. (1998).

7 SUMMARY AND DISCUSSION

We have proposed a global scenario for the formation and evolution of dSph galaxies, satellites of the MW, in their cosmological context using an improved version of the semi-analytical code GAMETE (Galaxy Merger Tree & Evolution, SSF07). This approach allows to follow self-consistently the dSph evolution and the MW formation and match, simultaneously, most of their observed properties. In this context dSphs formed within the Galactic environment, whose metallicity evolution depends on the history of star formation and mechanical feedback along the build-up of the Galaxy. The star formation and mechanical feedback efficiencies of dSphs are assumed to be the same as for all the Galactic building blocks; they are calibrated to reproduce the observable properties of the MW.

DSph candidates are selected among the MW progenitors following a dynamical and a reionization criteria; we choose haloes with masses (i) $M_4 < M < M_{2\sigma}$ if $z > z_{\text{rei}}$, (ii) $M_{30} < M < M_{2\sigma}$ if $z < z_{\text{rei}}$ i.e. we assumed the formation of galaxies with circular velocity $v_c < 30$ km/s to be suppressed after reionization, where $5.5 < z_{\text{rei}} < 10$ (Choudhury & Ferrara 2006). As the number of dSph candidates found varies with z_{rei} , we determine the fraction that will become MW satellites requiring that their number matches the observed one (~ 15). Once formed, dSphs are assumed to evolve in isolation with respect to the merging/accreting Galaxy. In this work we present the results obtained assuming $z_{\text{rei}} = 6$. This value provides a good agreement between the Sculptor MDF and the simulated one and gives a total number of dSph candidates of $N_{\text{tot}} \sim 200$; hence, we suppose that $\sim 10\%$ of them become MW satellites.

The results of our model, supported by the comparison with observational data and previous theoretical studies, allow to sketch a possible evolutionary scenario for dSphs. In our picture dSph galaxies are associated with Galactic progenitors corresponding to low-sigma density fluctuations ($M_4 < M < M_{2\sigma}$), that virialize from the MW environment before the end of reionization, typically when $z = 7.2 \pm 0.7$. Their total (dark+baryonic) mass results to be $M = (1.6 \pm 0.7) \times 10^8 M_\odot$.

At the virialization epoch the dSph birth environment is naturally pre-enriched due to previous SN explosions up to $[\text{Fe}/\text{H}]_{\text{GM}} \gtrsim -3$, a value fully consistent with that inferred from observations by Helmi et al. (2006). The subsequent dSph evolution is strongly regulated by mechanical feedback effects, more intense in low mass objects (MacLow & Ferrara 1999). We take winds driven by SN explosions to be metal enhanced ($Z^w = 10 Z^{\text{ISM}}$) as also confirmed by numerical simulations (Fujita et al. 2004) and by the X-ray observations of the starburst galaxy NGC1569 (Martin et al. 2002). Typically, ~ 100 Myr after the virialization epoch a complete blow-away of the gas caused by mechanical feedback is predicted. The 99% of the present-day stellar mass, $M_* = (3 \pm 0.7) \times 10^6 M_\odot$, is expected to form during the first 100 Myr. The stellar content of dSphs is then dominated by an ancient stellar population (> 13 Gyr old), consistent with

the analysis of the dSph CMD diagrams by Dolphin et al. (2005).

After the blow-away the galaxy remains gas-free and SF is stopped. Fresh gas returned by evolved stars allows to restart the SF ~ 150 Myr after the blow-away. The SFR, however, is drastically reduced due to the paucity of the returned gas. Mass loss from evolved stars has been also invoked by Carignan et al. (1998) to explain the detection of HI in the Sculptor dSph. About ~ 100 Myr later, a second blow-away occurs and the cycle starts again. Such intermittent SF activity is similar to those observed in Carina by Smecker-Hane et al. (1994) and to the one derived by Stinson et al. (2007) using numerical simulations. Roughly 1 Gyr after the virialization this bursts-like SFH ends while the SF activity proceeds until the present-day with a rapidly decreasing rate. At $z = 0$ the dSph gas content is $M_g = (2.68 \pm 0.97) \times 10^4 M_\odot$.

Our model allows to match several observed properties of Sculptor dSph:

- The Metallicity Distribution Function (Helmi et al. 2006). The pre-enrichment of the dSph birth environment accounts for the lack of observed stars with $[\text{Fe}/\text{H}] < -3$, a striking and common feature of the four dSph galaxies observed by Helmi et al. (2006).
- The stellar Color Magnitude Diagram (Tolstoy et al. 2003) and the decrement of the stellar $[\text{O}/\text{Fe}]$ abundance ratio for $[\text{Fe}/\text{H}] > -1.5$ (Gaisler et al. 2005, Shetrone et al. 2003). The agreement found between models and observations support the SFH we have predicted.
- The DM content $M = (3.4 \pm 0.7) \times 10^8 M_\odot$ and the high mass-to-light ratio $(M/L) = 158 \pm 33$ recently derived by Battaglia (2007), Battaglia et al. (2008); we find $(M/L) \sim 150$ using the predicted dark matter to stellar mass ratio and assuming $(M/L)_* = 3$.
- The HI gas mass content. The value derived by radio observations ($M_{\text{HI}} > 3 \times 10^4 M_\odot$, Carignan et al. 1998) is in agreement with our findings.

Interestingly, the model can also be used to put an upper limit on epoch of reionization, $z_{\text{rei}} < 8.5$. The total number of selected dSph candidates in fact, is reduced below the observed one ($N_{\text{tot}} \sim 5$) if $z_{\text{rei}} = 8.5$. In addition, the imprint of reionization lies in the suppression of dSphs formation below the reionization redshift, $z_{\text{rei}} = 6$. This result is fully consistent with the presence of an ancient stellar population (> 13 Gyr old) in *all* the observed dSph galaxies (Grebel & Gallagher 2004).

Despite the success of the model in producing a coherent physical scenario for the formation of dSphs in their cosmological context and matching several of the Sculptor and MW properties, several aspects deserve a closer inspection. Although Sculptor represents the best template to compare with because of its average properties and the large amount of available data, examples of deviations are already known. In particular the SFHs differ considerably among dSph galaxies (Dolphin et al. 2005, Grebel & Gallagher 2004). The Fornax CMD diagram, for example, indicates a massive presence of younger stars than in other dSphs (Dolphin et al. 2005; Stetson et al. 1998; Buonanno et al. 1999); the peculiarity of this object is also evident in the observed MDF, which is a monotonically increasing function up to $[\text{Fe}/\text{H}] \sim -1$ (Pont et al. 2004; Helmi et al. 2006; Battaglia

et al. 2006). The dSph properties inferred in our model, including the SFH and the MDF, are instead “Universal”. This is a consequence of the selection criteria, that gives a Universal dSph host halo mass, and of the assumed cosmological gas fraction in all virializing haloes. Since $M_4(z) < M_{2\sigma}$ only for $z < 9$ (see Fig. 1, right panel) and the typical mass of newly virializing halo is $\sim M_4(z) < M_{30}$, dSphs are forced to form in the redshift range $6 < z_{\text{rei}} < 9$. Due to the small variation of $M_4(z)$ in such a range, the dSph dark matter content is very similar in all objects and equal to $\sim 10^8 M_\odot$.

A refinement of the reionization criterion should allow larger deviations from the average evolutionary trend without altering it and possibly allow reionization imprints to emerge in their SFHs. Cosmological simulations by Gnedin (2000) show in fact that after reionization the gas fraction in haloes below a characteristic mass-scale is gradually reduced compared to the cosmic value. If included in our model such prescription might allow to form, just after the reionization epoch, massive dSphs ($M \geq M_4(z = 6)$) with a lower initial gas-to-dark matter ratio. Since mechanical feedback depends on the available mass of gas powering the SF and on the halo binding energy, this should translate in a less efficient mechanical feedback and a consequent more regular SF activity. In particular, if blow-aways do not occur, the SF could proceed until the present day with a higher rate, allowing massive formation of younger and more Fe-rich stars. Alternatively, random episodes of mass accretion and/or merging with primordial composition haloes, can be invoked as external gas sources to power the SF at lower redshifts. Another physical mechanism, tidal stripping by the gravitational field of the Galaxy, might be invoked (Ibata et al. (2001); Mayer et al. (2004, 2006)) to explain the paucity of remnant gas in dSph, and perhaps as a mechanism of star formation suppression. In our model, we see no need to resort to such effect as the large majority of the gas is expelled by SN feedback within the first 100 Myr of dSph evolution (we recall that the amount of newly born stars after that time is only $\approx 1\%$ of the final stellar mass). Hence, by the time dSphs find themselves embedded in the MW gravitational potential, there is little gas left to be stripped.

Finally, we like to comment on some of the model assumptions that could affect the results of the present work. The most relevant one certainly resides in the perfect mixing approximation which determines the metallicity evolution of the dSph birth environment and therefore of the low $[\text{Fe}/\text{H}]$ tail of the dSph MDF. Our persisting ignorance on all the physical effects regulating such process cannot allow to improve this assumption at the moment. The problem, however, is partially alleviated by the spread of the GM metallicity evolution (Fig. 1, middle panel) induced by the stochastic nature of the merger histories, which appears to be similar to what found by sophisticated numerical simulations of mixing in individual galaxies (Mori & Umemura 2006). DSph galaxies formed out of a metal-poor birth environment $[\text{Fe}/\text{H}] < -3$ are found in our model; however, their number is very small and their statistical impact on the average MDF negligible. Finally, the assumed PopIII IMF (here a δ -function centered in $m_{\text{PopIII}} = 200 M_\odot$) might in principle affect the chemical evolution of the MW environment given the large iron production of massive stars (see also SSF07 for a more detailed description). A comparison of results obtained using PopIII masses in the range $(140 - 260) M_\odot$ and

a Larson IMF, shows that the GM evolution is independent of the assumed PopIII IMF below $z = 10$. The dSph birth environment is therefore not affected by this hypothesis. We refer the reader to SSF07 for a detailed analysis of the PopIII IMF impact on the Galactic halo MDF.

ACKNOWLEDGEMENTS

We are grateful to G. Battaglia, N. Gnedin, E. Grebel, A. Helmi, E. Tolstoy and K. Venn for providing us their data and enlightening discussions. This work has made use of the IAC-STAR Synthetic CMD computation code. IAC-STAR is supported and maintained by the computer division of the Instituto de Astrofísica de Canarias. We are grateful to DAVID** members for discussions.

REFERENCES

- Aparicio A., Gallart C., 2004, *AJ*, 128, 1465
 Barkana R., Loeb A., 2001, *Phys. Rep.*, 349, 125
 Battaglia G. et al., 2006, *A&A*, 459, 423
 Battaglia G., 2007, Phd Thesis, University of Groningen, The Netherlands
 Battaglia G., Helmi A., Tolstoy E., Irwin M. J., in preparation
 Beers T. C., Christlieb N., 2006, private communication
 Bertelli G., Bressan A., Chiosi C., Fagotto F., Nasi E., 1994, *A&A*, 106, 275
 Binney J., Merrifield M., 1998, *Galactic Astronomy*. Princeton Univ. Press, Princeton
 Bond J. R., Cole S., Efstathiou G., Kaiser N., 1991, *ApJ*, 379, 440
 Bromm V., Ferrara A., Coppi P. S., Larson R. B., 2001, *MNRAS*, 328, 969
 Bromm V., Loeb A., 2004, *New Astron.*, 9, 353
 Bullock J. S., Kravtsov A. V., Weinberg D. H., 2001, *ApJ*, 548, 33
 Buonanno R., Corsi C. E., Castellani M., Marconi G., Fusi Pecci F., Zinn R., 1999, *AJ*, 118, 1671
 Carignan C., Beaulieu S., Cote S., Demers S., Meteo M., 1998, *ApJ*, 116, 1690
 Choudhury T. R., Ferrara A., 2006, *MNRAS*, 371, L55
 Christlieb N., et al., 2002, *Nat*, 419, 904
 Christlieb N., Bessel M. S., Eriksson K., 2006, in preparation
 Christlieb N., 2007, private communication
 Ciardi B., Ferrara A., 2005, *Space Sci. Rev.*, 116, 625
 Cole S., Lacey C. G., Baugh C. M., Frenk C. S., 2000, *MNRAS*, 319, 168
 Diemand J., Madau P., Moore B., 2005, *MNRAS*, 364, 367
 Dolphin A. E., Weisz D.R., Skillman E.D., Holtzman J.A., 2005, to appear in ed. Valls-Gabaud D. & Chavez M., *Resolved Stellar Populations*, ASP Conf.Ser. [[arXiv:astro-ph/0506430](https://arxiv.org/abs/astro-ph/0506430)]
 Fenner Y., Gibson B. K., Gallino R., Lugaro M., 2006, *ApJ*, 646, 184
 Ferrara A., Tolstoy E., 2000, *MNRAS*, 313, 291
 Frebel A., Christlieb N., Norris J. E., Aoki W., Asplund M., 2005, *Nat*, 434, 871
 Fujita A., Mac Low M. M., Ferrara A., Meiksin A., 2004, *ApJ*, 613, 159
 Ganguly R., Sembach K. R., Todd T. M., Savage B. D., 2005, *ApJ*, 157, 251
 Geisler D., Smith V. V., Wallerstein G., Gonzales G., Charbonnel C., 2005, *AJ*, 129, 1428
 Gilmore G., Wilkinson M., Kleya J., Koch A., Evans N. W., Wyse R. F. G., Grebel E. K. et al., 2007, *Nucl. Phys. B*, in press ([astro-ph/0608528](https://arxiv.org/abs/astro-ph/0608528))
 Gnedin N. Y., 2000, *ApJ*, 542, 535
 Gnedin N. Y., Kravtsov A. V., 2006, *ApJ*, 645, 1054
 Grebel E. K., Gallagher III J. S., 2004, *ApJ*, 610, L89
 Heger A., Woosley S. E., 2002, *ApJ*, 567, 532
 Helmi A. et al., 2006, *ApJ*, 651, L121
 van den Hoek L. B., Groenewegen M. A. T., 1997, *A&A*, 123, 305
 Hurley-Keller D. A., Mateo M., Grebel E. K., 1999, *ApJ*, 523, 25L
 Kereš D., Katz N., Weinberg D. H., Davé R., 2005, *MNRAS*, 363, 2
 Kravtsov A. V., Gnedin O. Y., Klypin A. A., 2004, *ApJ*, 609, 482
 Ikuta C., Arimoto N., 2002, *A&A*, 391, 55
 Ibata R. A., Lewis G. F., Irwin M., Totten E., Quinn T., 2001, *ApJ*, 551, 295
 Lacey C., Cole S., 1993, *MNRAS*, 262, 627
 Lanfranchi G., Matteucci F., 2007, *A&A*, 468, 927
 Larson R. B., 1974, *MNRAS*, 169, 229
 Larson R. B., 1998, *MNRAS*, 301, 569
 Lejeune Th., Cuisinier F., Buser R., 1997, *A&A*, 125, 229
 Mac Low M.-M., Ferrara A., 1999, *ApJ*, 513, 1421
 Martin C., Kobulniky H., Heckman T., 2002, *ApJ*, 57413, 1421
 Mateo M., 1998, *ARA&A*, 36, 435
 Mayer L., Moore B., Quinn T., Governato F., Stadel J., 2002, *MNRAS*, 336, 119
 Mayer L., Mastropietro C., Wadsley J., Stadel J., 2006, *MNRAS*, 369, 1021
 Mets M., Kroupa P., 2007, *MNRAS*, 376, 387
 Mihos J. C., Hernquist L., 1996, *ApJ*, 464, 641
 Moore B., Diemand J., Madau P., Zemp M., Stadel J., 2006, *MNRAS*, 368, 563
 Mori M., Umemura M., 2006, *Nat*, 440, 644
 Mori M., Ferrara A., Madau P., 2002, *ApJ*, 571, 40
 Omukai K., 2000, *ApJ*, 534, 809
 Omukai K., Tsuribe T., Schneider R., Ferrara A., 2005, *ApJ*, 626, 627
 Pont F., Zinn R., Gallart C., Hardy E., Winnick R., 2004, *ApJ*, 1247, 840
 Read J. I., Pontzen A. P., Viel M., 2006, *MNRAS*, 371, 885
 Ripamonti E., Tolstoy E., Helmi A., Battaglia G., Abel T., 2007, *EAS Publications Series*, 24, 15
 Ricotti M., Gnedin N. Y., 2005, *ApJ*, 629, 259
 Salvadori S., Schneider R., Ferrara A., 2007, *MNRAS*, 381, 647
 Schneider R., Ferrara A., Natarajan P., Omukai K., 2002, *ApJ*, 571, 30
 Schneider R., Ferrara A., Salvaterra R., Omukai K., Bromm V., 2003, *Nat*, 422, 869
 Schneider R., Omukai K., Inoue A. K., Ferrara A., 2006, *MNRAS*, 369, 1437
 Schneider R., Salvaterra R., Choudhury T. R., Ferrara A., Buringa C., Popa L. A., 2007, *MNRAS*, submitted
 Sheltrone M., Venn K., Tolstoy E., Primas F., Hill V., Kaufer A., 2003, *AJ*, 125, 684
 Smecker-Hane T. A., Stetson P. B., Hesser J. E., Lehnert M. D., 1994, *AJ*, 108, 507
 Stinson G. S., Dalcanton J. J., Quinn T., Kaufmann T., Wadsley J., 2007, *ApJ*, 667, 170
 Stetson P. B., Hesser J. E., Smecker-Hane T. A., 1998, *Astronomical Society of the Pacific*, 110, 533
 Tassis K., Abel T., Bryan G. L., Norman M. L., 2003, *ApJ*, 587, 13
 Tolstoy E., 2004, *ApJ*, 617, L119
 Vader J. P., 1986, *ApJ*, 305, 669
 Venn K. et al., 2004, *AJ*, 128, 1177
 Volonteri M., Haardt F., Madau P., 2003, *ApJ*, 582, 559
 Woosley S. E., Weaver T. A., 1995, *ApJ*, 101, 181

** www.arcetri.astro.it/science/cosmology/index.html